

# Detecting Extrasolar Asteroid Belts Through Their Microlensing Signatures

Ethan Lake<sup>1</sup>★, Zheng Zheng<sup>1</sup>, and Subo Dong<sup>2</sup>

<sup>1</sup>*Department of Physics and Astronomy, University of Utah, 115 South 1400 East, Salt Lake City, UT 84112, USA*

<sup>2</sup>*Kavli Institute for Astronomy and Astrophysics, Peking University, Yi He Yuan Road 5, Hai Dian District, Beijing 100871, China*

15 May 2022

## ABSTRACT

We propose that extrasolar asteroid belts can be detected through their gravitational microlensing signatures. Asteroid belt + star lens systems create so-called “pseudo-caustics”, regions in the source plane where the magnification exhibits a finite but discontinuous jump. These features allow such systems to generate distinctive microlensing light curves across a wide region of belt parameter space and possess remarkably large lensing cross-sections. Sample light curves for a range of asteroid belt parameters are presented. In the near future, space-based microlensing surveys (e.g., WFIRST) may be able to discover extrasolar asteroid belts with masses of the order of  $0.1M_{\oplus}$ .

**Key words:** gravitational lensing: strong — gravitational lensing: micro — asteroids: general

## 1 INTRODUCTION

Gravitational microlensing has established itself as a valuable tool for detecting objects covering a wide range of mass (e.g., Paczynski 1986). Successful microlensing surveys began over two decades ago with target star fields in both the Galactic bulge (Udalski et al. 1993) and the Small and Large Magellanic Clouds (SMC and LMC; Alcock et al. 1993; Aubourg et al. 1993). As pointed out by Mao & Paczynski (1991), microlensing can be used to probe extrasolar planetary systems. Following the discovery of exoplanets through the microlensing technique (e.g., Bond et al. 2004; Udalski et al. 2005; Beaulieu et al. 2006), the number of detections has been steadily increasing into the several dozens (e.g., Kains et al. 2013; Gould et al. 2014; Suzuki et al. 2014; Batista et al. 2014). Owing to its sensitivity to low-mass planets and planets beyond the snow line, microlensing has emerged as an important method to detect and study exoplanets (e.g., Gaudi 2010). In addition, microlensing can also be applied to detect and characterize free-floating planets (Gaudi 2002; Sumi et al. 2011).

It has also been suggested that microlensing can lend itself to the observational study of various parts of the planet-formation process, like circumstellar discs around source stars (Zheng & Menard 2005) and lens stars (Hundertmark et al. 2009). In this paper, we propose to use microlensing to detect extrasolar asteroid belts around lens stars.

The observational study of extrasolar asteroid belts and debris discs has recently become an active field of study. Asteroid-belt and Kuiper-belt like analogs have been inferred around several extrasolar systems from the observed infrared excess of their host stars (e.g., Chen & Jura 2001; Beichman et al. 2005; Moerchen

et al. 2007; Chen et al. 2009; Backman et al. 2009; Moerchen et al. 2010), resulting from dust generated by collisions of asteroids. Multiple asteroid-sized objects have also been found to transit a white dwarf (e.g., Vanderburg et al. 2015; Croll et al. 2015). Residual timing variations in millisecond pulsars are proposed as originating from asteroid belts (e.g., Shannon et al. 2013). Determining the prevalence of extrasolar asteroid belts could shed insight into the planet formation process and even help estimate the frequency of extraterrestrial life (Martin & Livio 2013). Therefore, it would be valuable if we have complementary and effective methods to probe extrasolar asteroid belts around main sequence stars.

In this paper, we show that microlensing by the lens system composed of a star and an asteroid belt can be a promising method. Microlensing is useful in this regard because of its sensitivity to low-mass objects located near the Einstein ring radius, which is typically on the order of a few AU. We find that asteroid belt + star lenses produce a wide variety of so-called “pseudo-caustics”, loci in the source plane across which the magnification of a source has a finite jump (e.g., Evans & Wilkinson 1998; Rhie 2010; Lee & Kim 2014; Lake & Zheng 2015). A detailed investigation on the magnification properties for the general ring/belt+point lens has been presented in Lake & Zheng (2015). In this paper, we show that sources passing over the pseudo-caustics can leave unique signatures in the resulting microlensing light curves, which should be easily identifiable in upcoming observational surveys. Furthermore, the pseudo-caustics occupy a comparatively large region of the source plane, meaning that the lensing cross-section is significantly higher than in planetary microlensing events.

The structure of this paper is as follows. In Section 2, we recall key gravitational lensing equations and describe the pseudo-caustics that are formed by the lenses we consider. Section 3 is devoted to the presentation of model light curves for a few illustrative

★ Contact e-mail: lake@physics.utah.edu

cases. Finally, Section 4 consists of a summary and a discussion of our results.

## 2 MAGNIFICATION PROPERTIES OF BELT+STAR LENSES

### 2.1 Lensing equations

The lens system here is composed of a star and an asteroid belt. We consider lens models with both idealised narrow rings and more realistic wide belts, which exhibit qualitatively similar behaviors. In each model, the circularly symmetric ring/belt is centred at the star. We denote the distance between the observer and the lens (source) as  $D_L$  ( $D_S$ ) and the distance between the lens and source as  $D_{LS}$  ( $D_S = D_L + D_{LS}$ ). The belt is described by an inner radius  $a_i$  and an outer radius  $a_o$  ( $a_i = a_o = a$  in the case of a ring), the inclination angle  $i$  (i.e., the angle between the normal of the ring/belt plane and the line of sight direction), and the mass ratio  $q$  of the ring/belt to the central lens star. We express the angular position vectors in the image (lens) plane and source plane as  $\mathbf{r}_l = (x_l, y_l)$  and  $\mathbf{r}_s = (x_s, y_s)$ , respectively, with the origin being the position of the lens star and the  $x$ -axis oriented along the major axis of the projected ring/belt.

Throughout, we normalize all angular vectors and ring/belt sizes by the Einstein ring radius of the combined ring/belt+star system,

$$\theta_E = \sqrt{\frac{4GM}{c^2} \frac{D_{LS}}{D_L D_S}}, \quad (1)$$

where  $M = M_{\text{belt}} + M_{\text{star}}$  is the total mass of the lensing system. In the lens plane, the physical scale corresponding to  $\theta_E$  is

$$D_L \theta_E \approx 4 \left( \frac{D}{2\text{kpc}} \right)^{1/2} \left( \frac{M}{M_\odot} \right)^{1/2} \text{AU}, \quad (2)$$

where  $D$  satisfies  $1/D = 1/D_L + 1/D_{LS}$ .

The general lens equation is

$$\mathbf{r}_s = \mathbf{r}_l - \alpha(\mathbf{r}_l), \quad (3)$$

where  $\alpha(\mathbf{r}_l)$  is the normalized deflection angle caused by the lensing system for light rays at  $\mathbf{r}_l$  in the image plane. The deflection angle has the contributions from both the star and the ring/belt. Analytic expressions for the deflection angle  $\alpha(\mathbf{r}_l)$  and magnification  $\mu$  for the lenses we consider here can be found in [Lake & Zheng \(2015\)](#).

[Lake & Zheng \(2015\)](#) perform a study on the gravitational lensing properties with a system made of a point mass surrounded by a ring/belt and focus their discussions on examples with  $q = 1$ . We refer the readers to the above paper for details. In this paper, we present cases with low mass ratio that are more suitable for the study of extrasolar asteroid belts.

### 2.2 Pseudo-caustics

Key to understanding the behavior of gravitational lenses is the study of so called ‘‘caustic curves’’. The caustic set contains the points in the source plane where the magnification  $\mu$  for a point source is formally divergent and represents points where the determinant of the lens mapping Jacobian vanishes.

Normally, the magnification is a smooth function for sources located away from the caustics. However, the belt+star lens models considered here possess regions in the source plane dubbed

‘‘pseudo-caustics’’, where the magnification is finite but changes discontinuously. Pseudo-caustics have been studied before in lensing systems with singular isothermal density distributions (e.g., [Kovner 1987](#); [Wang & Turner 1997](#); [Shin & Evans 2008](#); [Rhie 2010](#); [Lee & Kim 2014](#)), where they were associated with regions where the image multiplicity changes by one. In the systems considered here, the pseudo-caustics can be associated either with regions where the image multiplicity changes (narrow ring case) or where an image of a source suddenly changes in size (wide belt case). They are found to possess a broad variety of morphologies across the parameter space of the models we consider. A more detailed analysis of the pseudo-caustics is presented in [Lake & Zheng \(2015\)](#).

Since the boundaries of the pseudo-caustics represent areas where the magnification map is non-differentiable, they can in principle be found by finding points in the source plane where  $|\nabla\mu| \rightarrow \infty$ . In practice, we perform an inverse ray-shooting calculation (e.g., [Schneider & Weiss 1986](#)) by shooting rays from a uniform grid in the lens plane and collecting them on a grid in the source plane. The magnification of a cell in the source plane is then computed by dividing the number of rays it collects by the number it would collect in the absence of the lens.

Figure 1 shows magnification maps in the source plane for a narrow ring with  $a = 1.3$  and  $q = 10^{-3}$  across a range of inclinations. The pseudo-caustics show up as the X-shaped features for the cases with high inclinations (e.g.,  $i \gtrsim 40^\circ$ ), which are fairly generic for the types of lenses we consider. The mass ratio  $q = 10^{-3}$  may be rather unrealistic for asteroid belts, but the morphologies of the pseudo-caustics do not change significantly when  $q$  is lowered (the primary change being in the width of the pseudo-caustics). The  $q = 10^{-3}$  case is used for the purpose of illustration here. When the inclination of the ring is low, the pseudo-caustic are subdued. As shown in [Lake & Zheng \(2015\)](#), the deflection by a face-on ring is zero for rays passing interior to the ring and is identical to that produced by a point of same mass at the centre for rays passing exterior to the ring. Therefore, for the case of a low mass ratio, the magnification map of the ring+star system is close to that of the central star. As the inclination of the ring increases, the limbs of the X-shaped feature fold down towards the  $x$ -axis and eventually merge when the ring is seen edge-on. For the edge-on case, the system exhibits some features degenerate with that of an equal-separation triple point-mass lens (e.g., [Daněk & Heyrovský 2015](#)).

We find that the pseudo-caustics are most pronounced for rings with semi-major axes at or slightly beyond the Einstein ring radii ( $1 \lesssim a \lesssim 2$ ), as is the case of caustics for planetary microlensing ([Gould & Loeb 1992](#)). When we widen the idealised narrow ring to a belt, the pseudo-caustics become smoother and ‘‘smeared out’’, although the effect is not too dramatic for moderate belt widths ( $\Delta a \lesssim 0.5$ ). For comparison, our own asteroid belt extends from  $\sim 2.2$  to  $\sim 3.2$  AU ([Petit et al. 2001](#)), which if considered as a lens around a sun-like star halfway between the Sun and the Galactic centre gives a dimensionless width of  $\Delta a \sim 0.25$ .

Finally, we note that the pseudo-caustics extend out radially to cover a wide region of the source plane. Therefore, any given source trajectory in the source plane has a high likelihood of pseudo-caustic crossing, implying a high asteroid belt lensing cross-section. The pseudo-caustic crossing leads to distinct features in the microlensing light curves as shown in § 3.

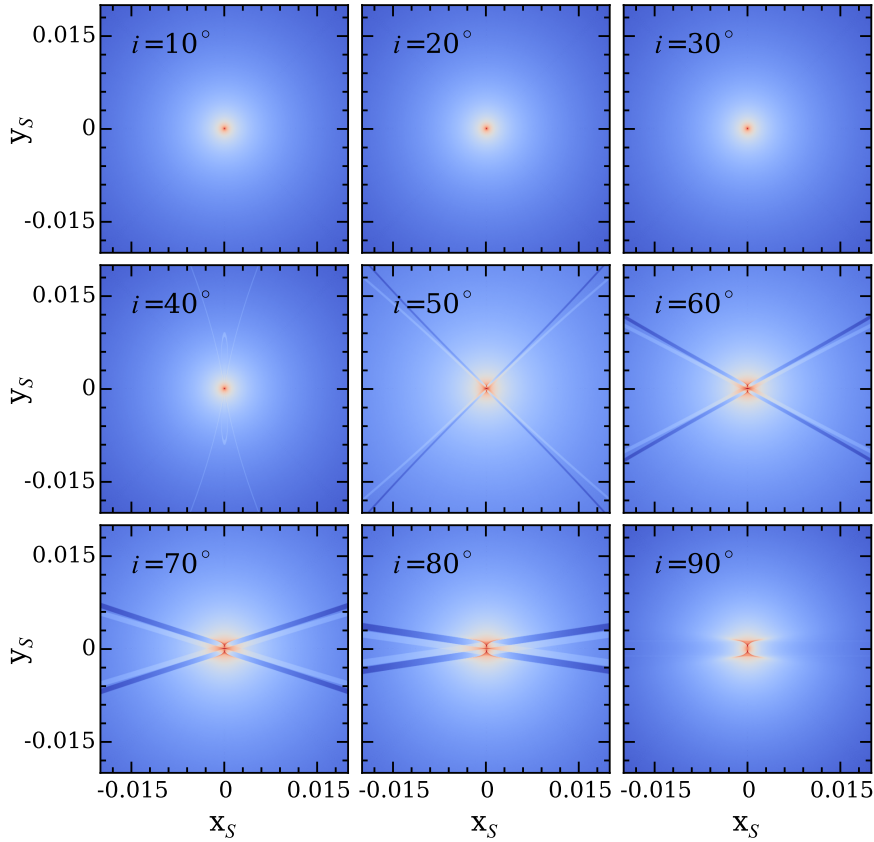


**Figure 1.** Magnification maps near the centre region in the source plane for a lens composed of a central star and a narrow ring with semi-major axis  $a = 1.3$  and mass ratio  $q = 10^{-3}$  across various inclinations. For low inclinations the ring acts as a point mass, and the perturbations it induces to the star’s magnification map are small. As the inclination passes  $\sim 45^\circ$ , an X-shaped pseudo-caustic feature appears. The dark regions indicate where the number of images produced by a source drops to one, with the lighter regions indicating where the number of images increases to three. As the inclination increases the limbs of the X fold down and become wider, eventually merging when the ring is seen edge-on. A source moving across these features generates a very distinctive light curve (see text for more details).

### 3 MODEL LIGHT CURVES

In this section, we present simulated light curves across a range of parameter combinations to demonstrate the expected behavior of belt+star microlensing events. Throughout this section, we assume the source star to be a  $0.3M_\odot$  M dwarf located near the Galactic centre with the belt+star lens located halfway to the Galactic centre, i.e. we set  $D_L = 4\text{kpc}$  and  $D_S = 8\text{kpc}$ . We take the lens star to be a sun-like star of mass  $M_{lens} = 1M_\odot$ , which gives  $\theta_E D_L \approx 4\text{AU}$ .

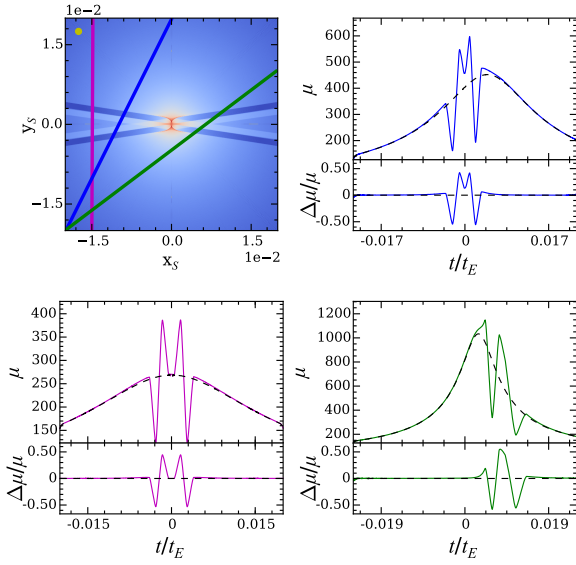
Figure 2 shows three model light curves for a narrow ring+star system with  $a = 1.3$ ,  $q = 10^{-3}$ , and  $i = 80^\circ$ . The case for lower mass ratio will be presented later, which has similar qualitative features. We focus on trajectories close to the centre, which lead to high magnification microlensing events. The top left panel shows the magnification map of the central region in the source plane, superimposed with the corresponding source trajectories for three light curves in the other three panels. The yellow circle at the top-left corner of the magnification map corresponds to the size of the source star, and we account for the finite source effect in calculating the light curves. In each light curve, the black dashed line shows the light curve for the star-only lens, with the bottom subpanel showing

the ratio of the ring+star light curve to the star-only one. Time is put in units of  $t_E$ , the Einstein radius crossing time. For a typical lens-source relative velocity of  $v_\perp = 110\text{ km s}^{-1}$ ,  $t_E$  is  $\sim 65$  days.

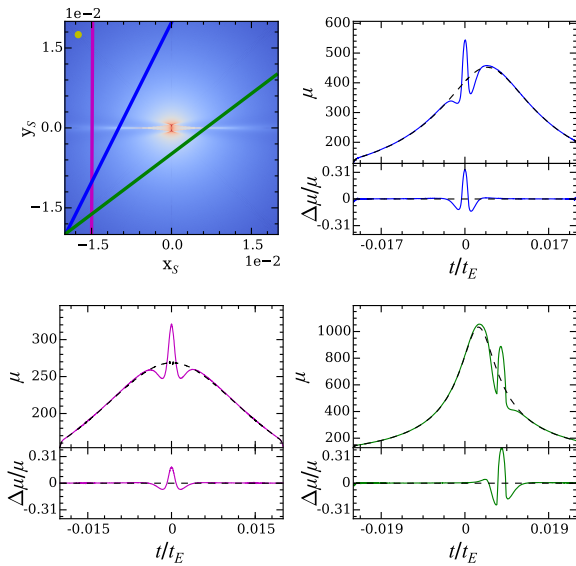
The distinct X-shaped pseudo-caustic feature in the magnification map shows up in each of the three light curves. Given the shape of the pseudo-caustics, the source has a high likelihood of crossing the pseudo-caustics twice, resulting in a light curve that exhibits a rapid decrease and increase in magnification, followed by a corresponding increase and decrease some time later. The maximum fractional change in magnification,  $\Delta\mu/\mu$ , can be as high as  $\sim 50\%$ . An observed light curve exhibiting these features would provide strong evidence for the presence of a ring+star lens.

Figure 3 is the same as Figure 2 but with  $a = 0.9$ . Lowering the semi-major axis of the ring folds the X-shaped feature down onto the  $x$ -axis and smoothens the pseudo-caustics. The maximum relative magnification  $\Delta\mu/\mu$  between the ring+star case and the star-only case decreases to 30%. In general, decreasing  $a$  even further results in a smaller perturbation to the star-only light curve.

Figure 4 shows the case with  $a = 1.3$  and  $i = 45^\circ$ . Reducing the inclination has the effect of “folding up” the X-shaped pseudo-caustics about the  $y$ -axis, and increasing the separation between the



**Figure 2.** Sample microlensing light curves for a lens with a central star and a narrow ring with semi-major axis  $a = 1.3$ , mass ratio  $q = 10^{-3}$ , and inclination  $i = 80^\circ$ . The top-left panel shows the magnification near the centre of the source plane. The circle at the top-left corner represents the dimensionless size of the source star. The other three panels show light curves corresponding to the given trajectories in the source plane, with the black dashed lines showing the light curve for the star-only case. The bottom sub-panels show the ratio of light curves of the star+ring case to the star-only case. The source is assumed to move along each trajectory in the top-left panel from bottom-left to top-right, with  $t = 0$  set at the halfway point of the trajectory.



**Figure 3.** Same as in Figure 2, but with  $a = 0.9$

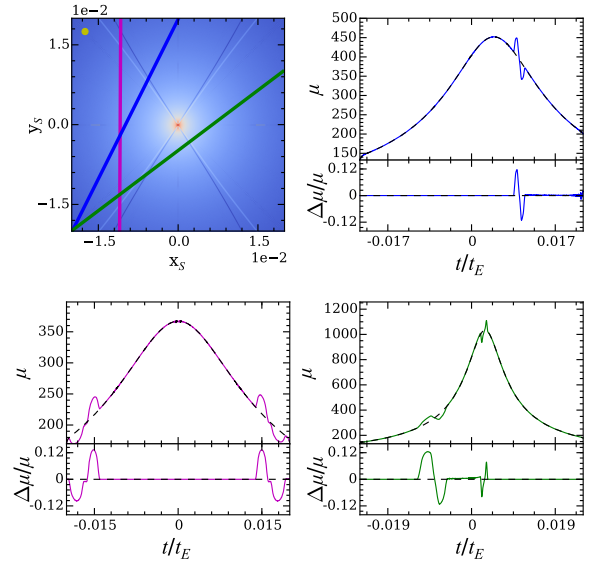


**Figure 4.** Same as in Figure 2, but with  $i = 45^\circ$ .

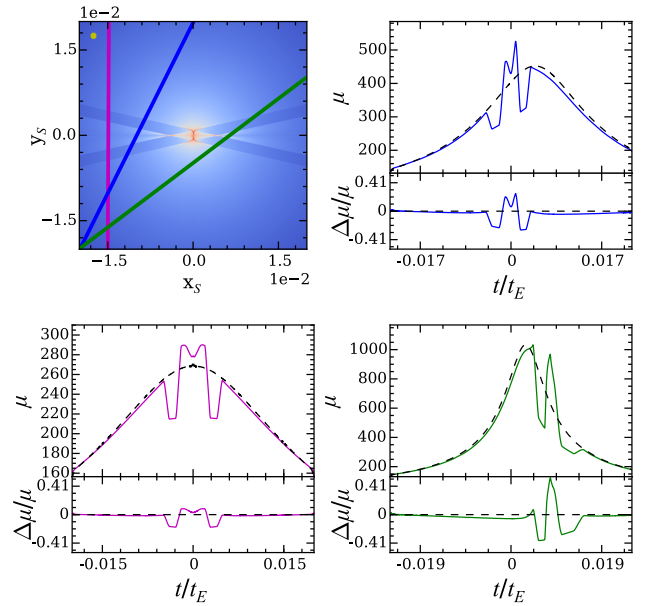


**Figure 5.** Same as in Figure 2, but with the ring replaced with a uniform belt with inner radius  $a_i = 1.0$  and outer radius  $a_o = 1.6$ . Widening the ring to a belt preserves the overall behavior of the light curve, but the perturbations to the star-only curve become smaller in magnitude with wider troughs.

high and low magnification areas of the pseudo-caustics. Additionally, the width of the pseudo-caustics becomes smaller and the perturbations to the star-only light curve decrease.

Figure 5 is again the same as Figure 2, but with the ring replaced by a uniform belt of inner radius  $a_i = 1.0$  and outer radius  $a_o = 1.6$ . If a belt of this width were placed around a sun-like lens star, a width of  $\Delta a = 0.6$  would correspond to a physical width of  $\sim 2.5$  AU. Thickening the ring smooths out the pseudo-caustics,

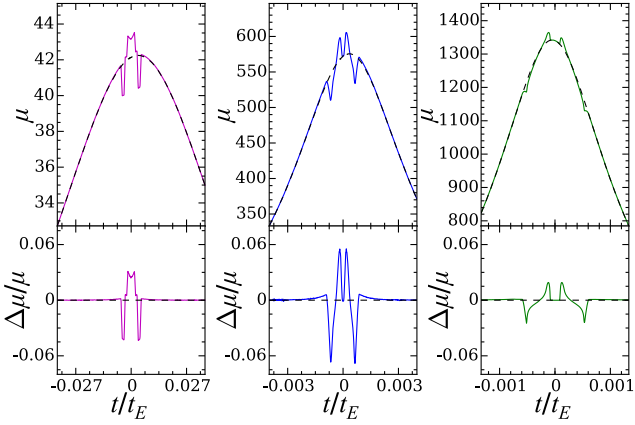


**Figure 6.** Three sample microlensing light curves for a lens composed of a star and a belt with  $q = 5 \times 10^{-5}$ ,  $i = 80^\circ$  and  $\Delta a = 0.25$  for different semi-major axes and source trajectories. From left to right, the belts are centred at  $a = 1, 1.2,$  and  $2,$  respectively. The dashed curves show the star-only case for comparison, with the bottom panels showing the ratio of the light curves of the belt+star to the star-only case. We assume a typical M dwarf source star located in the Galactic centre. Note that each light curve exhibits the same characteristic alternating magnification pattern despite having different peak magnifications.

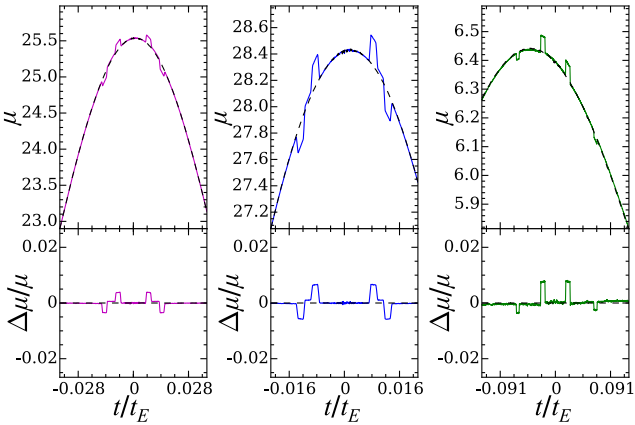


**Figure 7.** Three more sample microlensing lightcurves for a lens composed of a central star and a belt with  $q = 10^{-5}$  and  $i = 80^\circ$ . In the left, middle, and right panel, the belt is centred at  $a = 1.1, 1.6,$  and  $1.3,$  respectively, all with a width  $\Delta a = 0.3$ . All trajectories are at relatively large distances from the central star. These examples demonstrate that the large cross-sectional area of the pseudo-caustics allows them to leave signatures even in relatively low-magnification events.

with the light curves retaining their overall shape but possessing slightly more subdued peaks and flatter troughs.

In Figure 6 we present three sample light curves for different trajectories for a system with a lower belt-to-star mass ratio,  $q = 5 \times 10^{-5}$ , which corresponds to a belt mass of  $\sim 5M_\oplus$  for an M-dwarf lens star. The inclination of the belt is fixed at  $i = 80^\circ$ . From the left to right panel, the belts are centred at  $a = 1, 1.2,$  and  $2,$  respectively, with width  $\Delta a = 0.25$ . While the characteristic shape of the perturbations caused by the belt remains similar to the previous cases, the fractional change in magnification drops to a level of a few percent. Approximately, the fractional perturbations with

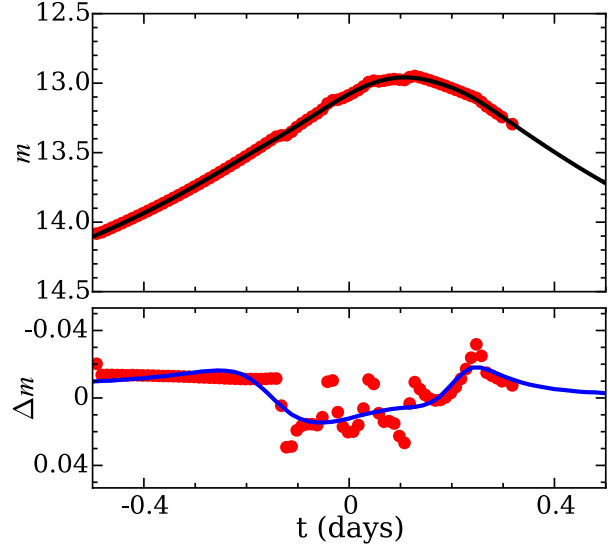


**Figure 8.** An example of fitting a sample belt+star light curve with a planet+star lens model. The top panel shows the belt+star light curve (red dots) plotted against the best-fitting single lens model (black curve), shown in magnitudes. The bottom panel shows the difference between the belt+star light curve and the best-fitting single lens model (red dots) compared to the difference between the best-fitting planet+star lens model and the best-fitting single lens model (blue curve).

respect to the star-only light curve are proportional to the mass ratio  $q$ , of the order of  $0.5(q/10^{-3})$ .

Finally, in Figure 7 three more sample light curves are presented for  $q = 10^{-5}$  and for relatively low magnification events, where the trajectory of the source star lies at large  $r_s$ . The inclination is again fixed at  $i = 80^\circ$  and the belts are centred at  $a = 1.1, 1.6,$  and  $1.3,$  with  $\Delta a = 0.3$  throughout. The characteristic pseudo-caustic crossing features caused by the belt clearly show up, with the relative magnification dropping to sub-percent levels.

Overall, microlensing events from belt+star lenses can be generically characterized by a rapid decrease and increase in magnification followed by a reversed increase and decrease in magnification, caused by the perturbation from the asteroid belt. Such a semi-symmetric feature is seen across a wide range of belt semi-major axes, belt widths, belt inclinations, belt-to-star mass ratios, and source trajectories, making it a robust observational signal. Such a feature is not usually seen in the light curves generated by other types of lensing systems, except a moderate degeneracy with an equal-separation triple point-mass lens when the belt is seen nearly edge-on.

The feature is distinct from that produced by planet microlensing. Observationally, it would be unlikely for a belt+star microlensing event to be misidentified as a planet+star one. To establish this quantitatively, we perform tests by fitting belt+star microlensing curves with a planet+star lens model. We produce theoretical belt+star microlensing light curve data and add photometric errors of 5 mmag (reasonable for the best ground-based microlensing surveys for high-magnification events). We then employ the method in Dong et al. (2009) to explore the parameter space of a planet+star lens system to model the data. Figure 8 shows an example, taken from a lens model with a belt of width  $\Delta a = 0.2$  centered at  $a = 1.25$  and with  $i = 80^\circ$ ,  $q = 10^{-5}$ . In the top panel, the points are the densely sampled light curve of the belt+star lens system, and the black curve is the best-fit from a single lens model. The bottom

panel shows the residuals to the best-fitting single lens model as well as the difference between the best-fitting planet+star model and the best-fitting single lens model (in blue). The planet+star model tends to fit the broad deviations from the single-lens model but fails to account for the small structures caused by the belt+star lens. The  $\chi^2$  difference between the planet+star and belt+star models is 215.7 for 902 degrees of freedom (i.e.,  $5.1\sigma$ ). For future applications, a systematic investigation on the differences in planet+star, belt+star, and planet+belt+star lens systems will be helpful.

#### 4 SUMMARY AND DISCUSSION

We investigate detecting extrasolar asteroid belts around stars through microlensing. Existence of asteroid belts leaves distinct signatures in microlensing light curves. Belt+star lenses generically create so-called “pseudo-caustics”, regions in the source plane where the magnification of a source is finite but changes discontinuously. The cross-section for pseudo-caustic crossing events is large for a wide range of belt configurations. In the light curves for most source trajectories, the X-shaped pseudo-caustics lead to a rapid rise and fall (or fall and rise), followed by a subsequent reversed fall and rise (or rise and fall). Such a characteristic, semi-symmetric feature can be used to identify belt+star microlensing events.

The width of the pseudo-caustic for systems with mass ratio  $q = 10^{-3}$  is about  $10^{-3}$  times the Einstein ring radius and decreases with decreasing mass ratio. For comparison, an M dwarf near the Galactic centre has a dimensionless radius of  $3 \times 10^{-4}$ . This means that the magnification jump caused by a pseudo-caustic crossing is smeared out by the finite source effect, which ultimately limits the sensitivity to detect extrasolar asteroid belt systems. This means that sources at large distances (large values of  $D_S$ ) are ideal, and that surveys should target main sequence source stars rather than giants, as has been pointed out by [Bennett & Rhie \(1996\)](#). Detecting asteroid belts with  $q \lesssim 5 \times 10^{-6}$  for sources near the Galactic centre is an approximate lower bound for the masses of belts that are likely to be observed. The same type of sources appear to be  $\sim 7$  times smaller if located in the LMC. Targeting stars in the LMC would therefore enable us to detect lower mass asteroid belts, although most upcoming surveys (i.e., WFIRST; [Spergel et al. 2015](#)) are being designed to target the Galactic bulge.

The small width of the pseudo-caustics in the source plane also means that pseudo-caustic crossing events only last for a short period of time (e.g., minutes to hours for Galactic centre sources). The required high cadence rates for detection are similar to those in current surveys like MOA and OGLE ([Sumi 2010](#); [Udalski et al. 2015](#)). As a concrete example for future surveys, we consider the photometric survey towards the Galactic bulge by the WFIRST satellite. With a 52s exposure, the photometric precision in a broad  $H$  band is about  $\sigma(H) \sim 10^{2/15(H-15)}$  mmag ([Gould et al. 2015](#)), where  $H$  is the apparent magnitude of the source. A  $0.3M_\odot$  M dwarf source star (with absolute magnitude  $M_H \sim 7.05$  mag; [Henry & McCarthy 1993](#)) in the Galactic centre has an apparent magnitude  $H \sim 21.57$  mag, and the corresponding photometric precision is  $\sim 7.5$  mmag. So even for microlensing events with moderate magnifications, percent level features caused by extrasolar asteroid belts in the light curves can be detected with high significance.

While microlensing features by extrasolar asteroid belts can be detected at high precision, one may wonder whether or not asteroid belts similar to the idealised ones considered here actually exist. Clearly the key parameter here is the mass ratio  $q$  of the as-

teroid belt to its parent star. The present mass of our own asteroid belt is only  $\sim 5 \times 10^{-4}M_\oplus$  ([Petit et al. 2001](#)), giving  $q \sim 5 \times 10^{-9}$  even for a  $0.3M_\odot$  M dwarf parent star. Observing such a low-mass belt would be very unlikely, even for a survey targeting the LMC to reduce the finite source effect. However, our asteroid belt is thought to have been several orders of magnitude more massive in the early years of our solar system, with a primordial mass of  $\sim 1M_\oplus$  before it lost most of its mass to ejection by interactions with other planets ([Weidenschilling 1977](#); [Petit et al. 2001](#)) over a time scale of a few Myr. For systems that lack massive planets orbiting near the belt, the lifetime of early, massive asteroid belts may be significantly longer. Cold planetesimal discs / asteroid belts of masses on the order of a few  $M_\oplus$  at a distance a few AU from a solar mass star can be dynamically stable over Gyr timescales ([Heng & Tremaine 2010](#)). There are hints from observations that massive asteroid belts or ring-like structures exist. For example, the inferred parent mass of the asteroid belt around the A-type star  $\zeta$  Leporis from the observation of dust emission a few AU from the star is about  $6.7 \times 10^{-2}M_\oplus$ , substantially more massive than our own one. Another example comes from the eclipse light curve of J1407 ([Kenworthy & Mamajek 2015](#)), which can be interpreted as caused by a companion star, J1407b, with a giant ring system ( $\sim 1M_\oplus$ , extending to a radius of  $\sim 0.6$  AU).

Overall, it is not unlikely that belt structures with masses of  $O(10)$  times the mass of the moon (corresponding  $q \gtrsim 2 \times 10^{-6}$  for a typical M dwarf host star) exist, which in principle can produce detectable microlensing features. The favorable configurations include a reasonably high inclination ( $i \gtrsim 75^\circ$ ) and a semi-major axis of  $a \gtrsim 1$ . It is natural to assume that most asteroid belts will have semi-major axes close to the snow line, beyond which the temperature from their parent stars is low enough to allow ices to form. This is encouraging, given that the snow line  $r_{\text{snow}} \approx 2.7(M/M_\odot)^{1/3}$  AU ([Martin & Livio 2013](#)) is fairly close to  $\theta_E D_L$  (around which the perturbations caused by the belt are most significant; see equation 2) for a typical Galactic microlensing event.

In our calculation of the microlensing signal, we assume a smooth disc or belt structure. In reality, a disc/belt is made of discrete bodies, and a smooth disc corresponds to the limit of small bodies. Depending on the mass distribution, discreteness effect in mass may need to be investigated and may need to be accounted for in modeling the microlensing light curve in observation.

All in all, it does not seem unreasonable to consider the existence of long-lived massive asteroid belts. If they exist, microlensing is an ideal method for observing them. Observational techniques are continuing to improve, with microlensing surveys reaching increasingly high levels of sensitivity. New space-based surveys like WFIRST will be able to detect Mercury-mass planets ([Spergel et al. 2013](#)) and will be well-poised to make the first detections of extrasolar asteroid belts, which will provide useful information on the formation of planets and dynamical evolution of asteroid belts.

#### 5 ACKNOWLEDGEMENTS

The work is partially supported by NSF grant AST-1208891. The support and resources from the centre for High Performance Computing at the University of Utah are gratefully acknowledged. S.D. is supported by the Strategic Priority Research Program “The Emergence of Cosmological Structures of the Chinese Academy of Sciences” (Grant No. XDB09000000) and Project 11573003 supported by NSFC.

**REFERENCES**

- Alcock C., et al., 1993, *Nature*, 365, 621  
 Aubourg E., et al., 1993, *Nature*, 365, 623  
 Backman D., et al., 2009, *ApJ*, 690, 1522  
 Batista V., et al., 2014, *ApJ*, 780, 54  
 Beaulieu J.-P., et al., 2006, *Nature*, 439, 437  
 Beichman C. A., et al., 2005, *ApJ*, 626, 1061  
 Bennett D. P., Rhie S. H., 1996, *ApJ*, 472, 660  
 Bond I. A., et al., 2004, *ApJ*, 606, L155  
 Chen C. H., Jura M., 2001, *ApJ*, 560, L171  
 Chen C. H., Sheehan P., Watson D. M., Manoj P., Najita J. R., 2009, *ApJ*, 701, 1367  
 Croll B., et al., 2015, preprint, ([arXiv:1510.06434](https://arxiv.org/abs/1510.06434))  
 Daněk K., Heyrovský D., 2015, *ApJ*, 806, 99  
 Dong S., et al., 2009, *ApJ*, 698, 1826  
 Evans N. W., Wilkinson M. I., 1998, *MNRAS*, 296, 800  
 Gaudi B. S., 2002, *ApJ*, 566, 452  
 Gaudi B. S., 2010, preprint, ([arXiv:1002.0332](https://arxiv.org/abs/1002.0332))  
 Gould A., Loeb A., 1992, *ApJ*, 396, 104  
 Gould A., et al., 2014, *Science*, 345, 46  
 Gould A., Huber D., Penny M., Stello D., 2015, *Journal of Korean Astronomical Society*, 48, 93  
 Heng K., Tremaine S., 2010, *MNRAS*, 401, 867  
 Henry T. J., McCarthy Jr. D. W., 1993, *AJ*, 106, 773  
 Hundertmark M., Hessman F. V., Dreizler S., 2009, *A&A*, 500, 929  
 Kains N., et al., 2013, *A&A*, 552, A70  
 Kenworthy M. A., Mamajek E. E., 2015, *ApJ*, 800, 126  
 Kovner I., 1987, *ApJ*, 312, 22  
 Lake E., Zheng Z., 2015, preprint, ([arXiv:0000.0000](https://arxiv.org/abs/0000.0000))  
 Lee D.-W., Kim S.-J., 2014, *MNRAS*, 443, 328  
 Mao S., Paczynski B., 1991, *ApJ*, 374, L37  
 Martin R. G., Livio M., 2013, *MNRAS*, 428, L11  
 Moerchen M. M., Telesco C. M., De Buizer J. M., Packham C., Radomski J. T., 2007, *ApJ*, 666, L109  
 Moerchen M. M., Telesco C. M., Packham C., 2010, *ApJ*, 723, 1418  
 Paczynski B., 1986, *ApJ*, 304, 1  
 Petit J.-M., Morbidelli A., Chambers J., 2001, *Icarus*, 153, 338  
 Rhie S. H., 2010, preprint, ([arXiv:1006.0782](https://arxiv.org/abs/1006.0782))  
 Schneider P., Weiss A., 1986, *A&A*, 164, 237  
 Shannon R. M., et al., 2013, *ApJ*, 766, 5  
 Shin E. M., Evans N. W., 2008, *MNRAS*, 390, 505  
 Spergel D., et al., 2013, AFTA Final Report,  
 Spergel D., et al., 2015, preprint, ([arXiv:1503.03757](https://arxiv.org/abs/1503.03757))  
 Sumi T., 2010, in Coudé du Foresto V., Gelino D. M., Ribas I., eds, *Astronomical Society of the Pacific Conference Series Vol. 430, Pathways Towards Habitable Planets*. p. 225  
 Sumi T., et al., 2011, *Nature*, 473, 349  
 Suzuki D., et al., 2014, *ApJ*, 780, 123  
 Udalski A., Szymanski M., Kaluzny J., Kubiak M., Krzeminski W., Mateo M., Preston G. W., Paczynski B., 1993, *Acta Astronomica*, 43, 289  
 Udalski A., et al., 2005, *ApJ*, 628, L109  
 Udalski A., Szymański M. K., Szymański G., 2015, *Acta Astronomica*, 65, 1  
 Vanderburg A., et al., 2015, *Nature*, 526, 546  
 Wang Y., Turner E. L., 1997, *MNRAS*, 292, 863  
 Weidenschilling S. J., 1977, *Ap&SS*, 51, 153  
 Zheng Z., Menard B., 2005, *ApJ*, 635, 599